

Detailed Iron-Peak Element Abundances in Three Very Metal-Poor Stars*

JOHN J. COWAN,¹ CHRISTOPHER SNEDEN,² IAN U. ROEDERER,^{3,4} JAMES E. LAWLER,⁵
ELIZABETH A. DEN HARTOG,⁵ JENNIFER S. SOBECK,⁶ AND ANN MERCHANT BOESGAARD⁷

¹*Homer L. Dodge Department of Physics and Astronomy, University of Oklahoma, Norman, OK 73019;*
jjcowan1@ou.edu

²*Department of Astronomy and McDonald Observatory, The University of Texas, Austin, TX 78712;*
chris@verdi.as.utexas.edu

³*Department of Astronomy, University of Michigan, 1085 S. University Ave., Ann Arbor, MI 48109, USA;*
iur@umich.edu

⁴*Joint Institute for Nuclear Astrophysics – Center for the Evolution of the Elements (JINA-CEE), USA*

⁵*Department of Physics, University of Wisconsin-Madison, 1150 University Ave., Madison, WI 53706;*
jelawler@wisc.edu, eadenhar@wisc.edu

⁶*Department of Astronomy, University of Washington, Seattle, WA 98195, USA; jsoback@uw.edu*

⁷*Institute for Astronomy, University of Hawaii at Manoa, 2680 Woodlawn Drive, Honolulu, HI 96822, USA;*
boes@ifh.hawaii.edu

ABSTRACT

We have obtained new detailed abundances of the Fe-group elements Sc through Zn ($Z = 21-30$) in three very metal-poor ($[\text{Fe}/\text{H}] \approx -3$) stars: BD+03°740, BD−13°3442, and CD−33°1173. High-resolution ultraviolet *HST*/STIS spectra in the wavelength range 2300–3050 Å were gathered, and complemented by an assortment of optical echelle spectra. The analysis featured recent laboratory atomic data for number of neutral and ionized species for all Fe-group elements except Cu and Zn. A detailed examination of scandium, titanium, and vanadium abundances in large-sample spectroscopic surveys indicates that they are positively correlated in stars with $[\text{Fe}/\text{H}] < -2$. The abundances of these elements in BD+03°740, BD−13°3442, CD−33°1173, and HD 84937 (studied in a previous paper of this series) are in accord with these trends and lie at the high end of the correlations. Six elements have detectable neutral and ionized features, and generally their abundances are in reasonable agreement. For Cr we find only minimal abundance disagreement between the neutral (mean of $[\text{Cr I}/\text{Fe}] = +0.01$) and ionized species (mean of $[\text{Cr II}/\text{Fe}] = +0.08$), unlike most studies in the past. The prominent exception is Co, for which the neutral species indicates a significant overabundance (mean of $[\text{Co I}/\text{H}] = -2.53$), while no such enhancement is seen for the ionized species (mean of $[\text{Co II}/\text{H}] = -2.93$). These new stellar abundances, especially the correlations among Sc, Ti, and V, suggest that models of element production in early high-mass metal-poor stars should be revisited.

* Based on observations made with the NASA/ESA *Hubble Space Telescope*, obtained at the Space Telescope Science Institute (STScI), which is operated by the Association of Universities for Research in Astronomy, Inc. (AURA) under NASA contract NAS 5-26555. These observations are associated with program GO-14232. Some data presented in this paper were obtained from the Barbara A. Mikulski Archive for Space Telescopes (MAST). These data are associated with Program GO-7402. Other data have been obtained from the European Southern Observatory (ESO) Science Archive Facility. These data are associated with Programs 67.D-0439(A), 68.B-0475(A), 68.D-0094(A), and 095.D-0504(A). This research has also made use of the Keck Observatory Archive (KOA), which is operated by the W.M. Keck Observatory and the NASA Exoplanet Science Institute (NExScI), under contract with NASA. This work has also made use of data collected from McDonald Observatory of the University of Texas at Austin.

Keywords: atomic physics - abundance ratios - Galaxy: chemical evolution - stellar abundances - stellar nucleosynthesis

1. INTRODUCTION

The origin of the elements is one of the important questions in modern astrophysics. With the exception of a few elements formed in the big bang, most all elements are synthesized in stars. But astrophysical sites and nucleosynthetic conditions that produce individual, as well as groups of, elements vary widely. Of particular interest to nucleosynthesis studies are relatively metal-poor stars of the Galactic halo, whose abundance sets must have been generated by few prior massive star deaths.

In the early 2000's our group concentrated on determining accurate abundances of neutron-capture elements ($Z > 30$, hereafter n -capture), particularly the rare-earth (RE) elements in metal-poor halo stars, in an attempt to understand the origin of these elements (Cowan et al. 2019 and references therein). Our approach relied upon two major efforts. First, we obtained high resolution spectra, both in the visible and ultraviolet, utilizing both ground-based and space-based telescopes, to identify as many n -capture transitions as possible. Second, we used Wisconsin laboratory atomic physics studies to obtain precise transition probabilities and hyperfine/isotopic substructures to greatly increase the reliability of individual species abundances. This multi-year effort to produce accurate stellar n -capture elemental abundances culminated in Lawler et al. (2009) and Sneden et al. (2009), and references therein.

More recently we have turned attention to the iron-group elements ($Z = 21-30$), because their abundances in metal-poor stars can be directly compared to predicted outputs from massive star element donors. Such studies face difficulties. First, for many stars not all Fe-group elements are easily detectable with the available spectra of low metallicity stars. Secondly, even when elements can be detected, often only neutral-species transitions are available for analysis in typical ground-based spectra. The populations of Fe-group elements in warmer dwarfs and cooler red giants usually are dominated by the ionized species; therefore the elemental abundances are mostly based on results from the minority species. Thirdly, in many instances only a handful of lines are employed to derive individual elemental abundances. Finally, significant questions have been raised about whether local thermodynamic equilibrium (LTE) can adequately describe the ionization equilibrium, and large upward corrections have been proposed to LTE-based abundances from neutral species (e.g., Bergemann et al. (2010), Andrievsky et al. (2018) and Shi et al. (2018)).

Our group has been concentrating on improving the laboratory data for Fe-group neutral and singly-ionized transitions normalized with radiative lifetimes from laser induced fluorescence. Lines of interest to cool-star stellar spectroscopy are emphasized. Citations to individual papers within this series will be given in §3. In each study we have used the new atomic data to re-derive abundances in the solar photosphere and in the very metal-poor ($[\text{Fe}/\text{H}] \sim -2.2^1$) main sequence turnoff star HD 84937. This star has been chosen because of its brightness, well-known atmospheric parameters,

¹ We adopt the standard spectroscopic notation (Wallerstein & Helfer 1959) that for elements A and B, $[A/B] \equiv \log_{10}(N_A/N_B)_* - \log_{10}(N_A/N_B)_\odot$. We use the definition $\log \epsilon(A) \equiv \log_{10}(N_A/N_H) + 12.0$, and equate metallicity with the stellar $[\text{Fe}/\text{H}]$ value. Also, $\log \epsilon(X \text{ I})$ or $\log \epsilon(X \text{ II})$ are to be understood as an elemental abundance determined from the named species.

and availability of good high-resolution spectra over a very large wavelength range (see [Sneden et al. 2016](#), hereafter SN16).

In this paper we expand our analyses of the Fe-group elements to include three very metal-poor ($[\text{Fe}/\text{H}] \simeq -3$) stars, BD+03°740, BD−13°3442, and CD−33°1173. That study reported many have not been. This represents the first-ever study of the Fe group with recent, consistent neutral and ionized species lab data for elements Sc through Ni in such low-metallicity halo stars, which should provide probes of early Galactic nucleosynthesis.

Our three warm, main-sequence turnoff stars are well-known targets of low-metallicity chemical composition studies. Many high-resolution spectroscopic investigations have centered on questions about their Li abundances and isotopic ratios (e.g., [Ryan et al. 1999](#), [Bonifacio et al. 2007](#), [Hosford et al. 2009](#), and references therein). There have been few recent comprehensive abundance analyses, caused in large part by the extreme line-weakness of their optical spectra. A significant exception is the detailed study of 28 main-sequence, subgiant, and giant stars in the metallicity range $-3.7 \leq [\text{Fe}/\text{H}] \leq -2.5$ by [Lai et al. \(2008\)](#) with spectra that extended into the near-UV spectral domain ($\lambda \gtrsim 3100 \text{ \AA}$). That work included BD+03°740, for which [Lai et al.](#) reported abundances for 15 species of the 10 Fe-group elements. We will compare our results with those of [Lai et al.](#) in §3.

[Roederer et al. \(2018\)](#), hereafter Paper 1, derived model atmospheric parameters and metallicities from $\gtrsim 250$ Fe I and Fe II transitions in these stars. Here we present abundances for the other Fe-group elements. In §2 we introduce the high-resolution spectroscopic data sets analyzed for the three stars. New abundance determinations of several elements and summaries of recent results for other elements are given in §3 with final iron-peak elemental abundances listed in §4. Interpretation and discussion of the iron-peak data and abundances, particularly nucleosynthesis origins and production mechanisms, along with the implications for Galactic chemical evolution, are included in §5. Finally, a summary and conclusions are detailed in §6.

2. SPECTROSCOPIC DATA AND ANALYSES

The high resolution spectra for BD+03°740, BD−13°3442, and CD−33°1173 (hereafter called “program stars”) have been described in detail in Paper 1. Briefly, the spectra in the UV region (2290–3050 Å) were gathered with the Space Telescope Imaging Spectrograph (STIS; [Kimble et al. 1998](#); [Woodgate et al. 1998](#)) on board the *Hubble Space Telescope* (*HST*). The instrumental configuration was with the E230M echelle grating centered at $\lambda 2707$, the $0''.06 \times 0''.2$ slit, and the NUV Multianode Microchannel Array (MAMA) detector. The spectral resolving power was $R \equiv \lambda/\Delta\lambda \simeq 30000$. The *HST*/STIS spectra for the three program stars were obtained with STIS in Program GO-14232. See Paper 1 for discussion of the observations of HD 84937.

Optical spectra of these stars were obtained from online archives from the ESO Very Large Telescope Ultraviolet and Visual Echelle Spectrograph (UVES; [Dekker et al. 2000](#)), the Keck I Telescope High Resolution Echelle Spectrometer (HIRES; [Vogt et al. 1994](#)), and the McDonald Observatory Harlan J. Smith Telescope and Robert G. Tull Coudé Spectrograph ([Tull et al. 1995](#)). All stars have optical spectra with $R \gtrsim 40,000$ and wavelength coverage mostly complete in the 3050–6800 Å range. See Table 1 of Paper 1 for the characteristics of all the spectra used in our work.

3. ABUNDANCE DETERMINATIONS FOR BD+03°740, BD−13°3442, AND CD−33°1173

The analyses followed the methods used for our study of HD 84937 (SN16). Derivation of model atmospheric parameters was done with Paper 1 and will not be repeated here. We adopted the values from that paper for the program stars. For HD 84937 we used the model parameters from SN16. The parameters for these four stars are listed in Table 1. Stellar photospheric models with these parameters were interpolated from the Kurucz (2011) model grid² using software kindly provided by Andrew McWilliam and Inese Ivans.

In this study all line abundances were determined with interactive fits of observed and synthetic spectra. The linelists for generating the synthetic spectra were as described in SN16. Beginning with the Kurucz (2011) atomic and molecular line database³, we added/substituted/corrected the atomic spectral features that have been included in recent accurate laboratory data papers by the Wisconsin atomic physics and Old Dominion molecular physics programs (e.g., Yousefi & Bernath 2018, Lawler et al. 2019, and previous studies in those series).⁴ These linelists and the stellar atmospheric models were used by the LTE plane-parallel synthetic spectrum code MOOG (Snedden 1973). We used the code version that includes scattering in the continuum source function (Sobeck et al. 2011), although in our warm main-sequence turnoff stars the scattering contribution is very small even in the UV spectral region.

In Table 2 we list all the transitions used in our analyses, and the resulting abundances for the three program stars. Mean abundances in both $\log \epsilon$ and $[X/H]$ forms are given in Table 3, along with their line-to-line standard deviations. **However, Cu I and Zn I are represented by only two transitions each per star, and in several cases the species statistical σ values are unrealistically near 0.00. Therefore in such cases we have entered “(0.1)” for their standard deviations in Table 3.** The mean abundances and standard deviations are illustrated in Figure 1, along with the values for HD 84937 (taken from SN16).

As a general rule, we were able to detect the most lines for BD+03°740, the next most for BD−13°3442, and the fewest for CD−33°1173, approximately in order of increasing T_{eff} (which produces weaker-lined spectra for a given metallicity) and slightly decreasing signal-to-noise (S/N) ratios in the *HST*/STIS spectra of these stars. The abundances for HD 84937 in this table are quoted from SN16.

In our stars the Fe-group elements Sc through Ni ($Z = 21-28$) have many detectable ionized-species transitions, all of which have benefited from recent lab studies. Additionally, in the atmospheres of our stars these elements are almost completely ionized, as shown in Figure 2 of SN16. The neutral species account for at most a few percent of the elemental abundances. Therefore our primary Sc–Ni abundance sources will be the ionized species, while the neutrals will mainly serve as indicators of how well the basic Saha balances hold with our LTE analytical approach.

The only previous investigation of our stars to extensively examine their ionized-species transitions was that of Lai et al. (2008), who reported abundances for Fe-group ionized species of Sc, Ti, V, Cr, Mn, and Fe in BD+03°740. Our results to be discussed below generally are in good accord with theirs, with $\langle [X/Fe]_{\text{Lai08}} - [X/Fe]_{\text{thiswork}} \rangle = 0.02$ for 14 neutral and ionized species in common. We comment specifically on Cr in §3.1.4.

² <http://kurucz.harvard.edu/grids.html>

³ <http://kurucz.harvard.edu/linelists.html>

⁴ A code to accomplish this is available at <https://github.com/vmplacco/linemake>, along with all the transitions used by that code. A list of the laboratory studies contributing to this database can be found at <http://www.as.utexas.edu/chris/lab.html>.

3.1. *Comments on Individual Species*

Here we will discuss some analytical aspects of each of the Fe-group elements, generally deferring abundance interpretations to later sections.

3.1.1. *Scandium*

A new laboratory transition probability and hyperfine structure study for Sc I and Sc II has been published by Lawler et al. (2019). No Sc I lines in HD 84937 were detectable by SN16. Our program stars have similar temperatures and gravities to those of HD 84937 but $\simeq 0.7$ dex lower metallicities (Table 1). Thus it is not surprising that we failed to detect Sc I in these stars also. The series of Fe-group transition data papers has used HD 84937 as a test object for application to stellar spectra. Lawler et al. (2019) derived $\log \epsilon = 1.08$ ($\sigma = 0.05$) from 29 Sc II lines. This new value is identical to that given for HD 84937 in Table 3 from SN16.

3.1.2. *Titanium*

Transition probabilities for Ti I are from Lawler et al. (2013) and for Ti II are from Wood et al. (2013). These were also employed by SN16 for HD 84937. In the Wood et al. paper attention was brought to a dip in abundances from Ti II in the blue spectral region. For $\lambda > 3800 \text{ \AA}$ the HD 84937 mean abundance was $\log \epsilon = 3.12$ ($\sigma = 0.04$), in agreement with the mean value from Ti I lines. But for shorter wavelengths the Ti II lines yielded $\log \epsilon = 3.06$ ($\sigma = 0.09$), with the lowest values coming from lines with branching fractions greater than 0.2 in the wavelength region most affected by the Balmer continuum opacity ($\sim 3100\text{--}3650 \text{ \AA}$); see §7 of Wood et al., where this issue is discussed in detail without a clear resolution to the problem. This issue does not appear to be significant in our program stars, with a mean of the differences of the abundances from lines in the $3100\text{--}3800 \text{ \AA}$ range minus those from lines with wavelengths $>3800 \text{ \AA}$ being -0.07 dex (Table 3) compared to -0.06 dex in HD 84937. Our abundances from the ionized-species lines are $\simeq 0.10$ dex smaller than those from neutral-species ones, with CD-33°1173 having the largest species mismatch.

3.1.3. *Vanadium*

Using V II transition probabilities and hyperfine structure data from Wood et al. (2014a) we determined V abundances from 30–47 lines in the program stars. Their mean abundance is $\log \epsilon \simeq 1.5$, about 0.4 dex smaller than found for HD 84937 (Table 3). Unfortunately we could not check the ionization equilibrium for this element because we were unable to detect V I lines in any of our program stars. The neutral species has well-determined lab data for more than 800 lines (Lawler et al. 2014 and Wood et al. 2018), but application to HD 84937 by Lawler et al. resulted in only 10 useful transitions. Nine of these lines were illustrated in Figure 7 of that paper, revealing that nearly all of them have depths in that star much less than 10%. Scaling those depths by the V abundances found from the ionized species in our program stars suggests that the strongest V I lines probably would have depths $< 2\%$, thus rendering them undetectable in our spectra.

3.1.4. *Chromium*

The laboratory transition data for Cr I are taken from Sobek et al. (2007) and those for Cr II are from Lawler et al. (2017). The abundances derived from the ionized species are based on at least 50 lines for each star, and there is excellent line-to-line agreement ($\sigma \simeq 0.06$, Table 3). For Cr I there are fewer detectable lines (10–13), the scatter among them is somewhat larger ($\sigma \simeq 0.11$), and most

importantly the neutral-species mean abundances for the three stars are about 0.2 dex lower than those from the ionized species. This is an issue that has been discussed previously. Kobayashi et al. (2006) summarized the observational results at that time in their Figures 20 and 21, which suggested that, at $[\text{Fe}/\text{H}] \sim -3$, abundances from Cr I lines on average were ~ 0.4 dex lower than those from Cr II lines. Subsequent studies, e.g. Roederer et al. (2014a), have not relieved this problem.

For our stars on average the abundances derived from the neutral species are only $\simeq 0.15$ dex lower than those derived from the ionized species. We note that nearly half of the Cr I transitions used here arise from the ground state (Table 2), and they yield abundances about 0.1 dex lower than those from excited states ($\chi \simeq 1.0$ eV). Use of only the excited-state lines would bring reasonable agreement between Cr I and Cr II abundances. The NLTE computations of Bergemann et al. (2010) suggest that LTE abundances derived from the neutral species are too low in metal-poor stars while those derived from the ionized species are approximately correct. We concur, but lack the detailed information necessary to understand the excitation-state dependence noted here. Therefore we retain both Cr species as abundance indicators for our stars. A new NLTE investigation of this element would be welcome.

Finally, our Cr abundances are in excellent accord with those of Lai et al. (2008): they reported $[\text{Cr I}/\text{Fe}] = -0.07$ and $[\text{Cr II}/\text{Fe}] = +0.05$, while we derive -0.01 and $+0.08$, respectively. In total, for the 11 stars in their survey with both neutral and ion Cr abundances Lai et al. find a larger mean difference, $\langle [\text{Cr I}/\text{Fe}] - [\text{Cr II}/\text{Fe}] \rangle = -0.20$, but most of those stars are red giants, not main-sequence turnoff stars.

3.1.5. Manganese

Transition probabilities and hyperfine structure components for both Mn I and Mn II were taken from Den Hartog et al. (2011). Abundances for our stars derived from the ionized lines have low line-to-line and star-to-star scatter. For the neutral species only 3–4 transitions were detectable, of which three are the strong resonance lines at 4030.8, 4033.1, and 4034.5 Å. Studies of metal-poor stars routinely report significantly deficient Mn abundances, often $[\text{Mn}/\text{Fe}] \lesssim -0.5$ (e.g., Cayrel et al. 2004, Cohen et al. 2004, Yong et al. 2013, Roederer et al. 2014a). Bergemann & Gehren (2008) used detailed computations of Mn I line formation to argue that actual Mn deficiencies are only ~ -0.2 dex if departures from LTE are taken into account for low metallicity stars. However, their calculations indicated much larger NLTE corrections for the resonance lines, about +0.5 dex in total.

The contrast in LTE abundances between Mn I resonance and higher excitation lines was discussed in SN16 and illustrated in the lower panel of their Figure 6. The offset is consistent with that predicted by Bergemann & Gehren (2008). The abundance derived from Mn I lines in our program stars is $\simeq 0.2$ dex lower than that for Mn II (Table 3). Among the 16 neutral-species non-resonance lines used by SN16 for HD 84937, we can detect just two of them (3569.5 and 4041.4 Å; see Table 2) in our stars. These lines yield mean abundances of $\log \epsilon = 2.39$ in BD+03°740, 2.39 in BD−13°3442, and 2.24 in CD−33°1173. These values agree well with the Mn II mean abundances given in Table 3, with the caution that the 3569 and 4041 Å lines are only few percent deep in our stars.

Our results for the Mn I resonance lines, based entirely on LTE computations, have not been adjusted for suspected NLTE effects. We believe that the computations of Bergemann & Gehren (2008) are probably correct for the extra corrections needed for the resonance lines. Here we have chosen simply to accept the abundances from the higher-excitation Mn I transitions; see §4. This issue should be explored again in a future NLTE analysis.

3.1.6. *Iron*

Paper 1 explored Fe abundances in detail. Here we adopt its results for Fe I. More recently, [Den Hartog et al. \(2019\)](#) have determined new transition probabilities for Fe II, 122 of them in the UV ($\lambda < 3300 \text{ \AA}$) and 10 of them at longer wavelengths. See that paper for an extended discussion of these new *gf* values compared to those enumerated in the NIST ASD ([Kramida et al. 2018](#))⁵ and in the lab/solar empirical values for optical lines recommended by [Meléndez & Barbuy \(2009\)](#). In general, the [Den Hartog et al.](#) transition probabilities for blue multiplets of Fe II are lower by 0.0–0.1 dex than those from NIST, but they are in general agreement with those of [Meléndez & Barbuy](#). The values adopted in Paper 1 were from NIST. We used the [Den Hartog et al. \(2019\)](#) and [Meléndez & Barbuy \(2009\)](#) *gf*-values for determination of ionized-species abundances in our program stars. Our new Fe II abundances are higher by 0.15 dex than reported in Paper 1, creating an average small ion-neutral abundance offset of +0.1 dex.

3.1.7. *Cobalt*

Both Co I and Co II have recent lab transition probability and hyperfine structure analyses ([Lawler et al. 2015](#), [Lawler et al. 2018](#)). But application of these line data to the three program stars produces the most significant neutral/ion abundance clash of this study. The mean values, from Table 3, are $\langle [\text{Co I}/\text{H}] \rangle = -2.53$ while $\langle [\text{Co II}/\text{H}] \rangle = -2.93$, smaller by a factor of 2.5. In Figure 2 we illustrate the problem with a comparison of observed and synthetic spectra of BD+03°740 in a small UV region that contains several Co I and Co II lines. Inspection of this figure easily suggests that the abundances from neutral-species transitions are substantially larger than those from ionized-species ones. The Co I abundances for our stars are based on 28–36 lines, an order of magnitude more than most large-sample surveys. The Co II abundances are based on 16–21 lines, none of which have played significant roles in past Co studies except SN16.

Six elements (Ti, Cr, Mn, Fe, Co, and Ni) have abundances derived from both neutral and ionized species. Inspection of Table 3 and Figure 1 shows that for five of these elements the species abundances agree with each other to within ~ 0.2 dex, sometimes much better than that. The glaring exception in our stars is Co, for which $\langle \log \epsilon(\text{Co I}) - \log \epsilon(\text{Co II}) \rangle \simeq +0.4$.

Co has a prominent place in abundance studies of very metal-poor stars. For nearly three decades spectroscopic surveys have reported that for **metallicities in the range $-2.5 \lesssim [\text{Fe}/\text{H}] \lesssim +0.0$** **Co retains** its solar abundance ratio, $[\text{Co}/\text{Fe}] \simeq 0.0$, but for lower metallicities the Co relative abundance steadily (perhaps) increases, reaching $[\text{Co}/\text{Fe}] \sim +0.5$ at $[\text{Fe}/\text{H}] \sim -3.0$ (e.g., [Ryan et al. 1991, 1996](#), [McWilliam et al. 1995](#), [Cayrel et al. 2004](#), [Cohen et al. 2004](#), [Barklem et al. 2005](#), [Yong et al. 2013](#), [Roederer et al. 2014a](#)). Nearly all metal-poor star surveys have used only Co I transitions, as Co II features only become strong in the UV. Typically only a handful of Co I lines have contributed to the reported Co abundances in these papers. Additionally, NLTE computations by [Bergemann et al. \(2010\)](#) suggested that there may be large positive abundance corrections for Co I lines in very metal-poor stars, +0.5 dex or more. Their Figure 6 proposes that $[\text{Co}/\text{Fe}]_{\text{NLTE}} \sim +0.7$ for $[\text{Fe}/\text{H}] < -2$.

If we had studied only Co I in these stars, we would have confirmed the high Co from past investigations of very low metallicity stars. But neutral Co is just a trace species of Co in very metal-poor

⁵ Atomic Spectra Database of the National Institute of Standards and Technology; https://physics.nist.gov/PhysRefData/ASD/lines_form.html

main-sequence turnoff stars. For HD 84937, Figure 2 of SN16 suggests that $N_{\text{CoII}}/N_{\text{CoI}} \gtrsim 25$, meaning that more than about 95% of the element exists as singly-ionized Co. Bergemann et al. (2010) do not consider NLTE line formation for Co II in detail, but they suggest that the corrections to the LTE abundances in our types of stars will be small. Acceptance of the ionized-species abundance puts the relative [X/H] values for Co in agreement with those of its Fe-group element neighbors; i.e., the mean of [Co/Fe] in the target stars is approximately solar. We believe that the large abundances indicated by Co I are not correct.

3.1.8. Nickel

Wood et al. (2014b) presented laboratory transition probabilities⁶ for 371 Ni I transitions. With these new gf values, we obtained consistent results for our stars with a mean abundance $\log \epsilon = 3.40$, using 35–45 lines per star, with line-to-line scatters $\sigma \simeq 0.08$ (Table 3). Happily, the derived abundances from Ni II transitions is essentially in agreement, with a mean $\log \epsilon = 3.36$ in the three program stars. However, some cautions should be raised here: (a) only 7–8 ionized-species lines could be detected in our stars; (b) all of these lines are deep in the UV, $\lambda < 2500 \text{ \AA}$; (c) the abundance scatters are large, $\sigma \simeq 0.16$; and (d) perhaps most importantly, Ni II laboratory gf values have not been revisited recently. Wood et al. (2014b) adopted the transition probabilities of Fedchak & Lawler (1999) and they have been used in our analysis. Since Ni is the heaviest Fe-group element with detectable neutral- and ionized-species transitions in very metal-poor stars, a new laboratory Ni II lab study would be worthwhile.

3.1.9. Copper

The available transitions are severely limited here. All strong Cu II lines occur well shortward of our 2300 \AA *HST*/STIS wavelength limit. Of the possible Cu I transitions, we were only able to work with the resonance lines at 3247.5 and 3273.9 \AA . The transitions at 5105.5 and 5782.1 \AA , used in most stellar Cu abundance studies, are far too weak for detection in our stars. From the resonance lines in the three program stars, we derived a mean abundance of $\langle \log \epsilon \rangle \simeq 0.6$, or $\langle [\text{Cu}/\text{H}] \rangle \simeq -3.5$. However, it is possible that these very low abundances may be severe underestimates, as some studies (e.g., Andrievsky et al. 2018, Shi et al. 2018) have argued that LTE-based abundances should be corrected upward by large factors, typically by at least +0.5 dex in very metal-poor stars.

Some information on stellar abundances from Cu II now is available. For two metal-poor ($[\text{Fe}/\text{H}] \simeq -2.4$) red giants, Roederer et al. (2014b) employed four Cu II lines in the 2030–2130 \AA spectral range to determine $[\text{Cu}/\text{H}] \simeq -2.8$. More directly, for HD 84937 Roederer & Barklem (2018) used these same Cu II features, deriving $[\text{Cu}/\text{H}] = -2.75$. **We have added their Cu II abundance to the bottom panel of Figure 1.** The abundances from neutral lines for this star are $[\text{Cu}/\text{H}] \simeq -3.2$ (SN16) and $[\text{Cu}/\text{H}] \simeq -3.1$ (Roederer & Barklem). The 0.3–0.4 dex larger abundance from Cu II lines suggests that NLTE corrections of this magnitude probably should be applied to our Cu I results. However, we lack ionized-line abundances in our program stars, which are significantly more metal-poor than those studied by Roederer et al. (2014b) and Roederer & Barklem, and our spectra do not cover the shorter UV wavelengths where the Cu II lines are found. Therefore we have

⁶ Additionally, this paper considered isotopic wavelength splitting from the five stable Ni isotopes. However, isotopic shifts for Ni I only become large enough to materially affect line shapes in the red spectral region, $\lambda > 6000 \text{ \AA}$. This line complexity is negligible in our stars, which have no detectable transitions in the red.

chosen here not to make arbitrary adjustments to our LTE-based abundances, but just as in the cases of Cr I and Mn I we urge a comprehensive NLTE study of Cu I and Cu II for our program stars.

3.1.10. Zinc

Zn II features are found at UV wavelengths shorter than those covered by our STIS spectra. (The resonance lines of this species occur at 2025.5 and 2062.0 Å.) As in the case of Cu, we can only detect the Zn I resonance lines at 3302.6 and 3345.0 Å; all higher-excitation lines of the neutral species are absent in our spectra. The 3302 and 3345 Å lines are extremely weak, and in fact they cannot be detected in CD-33°1173.

Support for the Zn I results comes from the literature studies discussed for Cu in §3.1.9. The Zn I and II lines in the two metal-poor red giants studied by Roederer et al. (2014b) yielded overabundances $[\text{Zn}/\text{Fe}] \simeq +0.3$, comparable to those of our program stars. The Roederer & Barklem (2018) abundances for neutral and ionized Zn lines in HD 84937 are $[\text{Zn}/\text{Fe}] = +0.23$ and $+0.13$, respectively, while SN16 reported $[\text{Zn}/\text{Fe}] = +0.16$ from just the neutral lines in this star. **Their abundance for Zn II has been entered into the bottom panel of Figure 1.** This limited sample of Zn II abundances suggests that Zn I features yield reliable abundances in this metallicity regime. $[\text{Zn}/\text{Fe}]$ overabundances appear to be real.

4. FINAL ABUNDANCES FOR THREE VERY LOW METALLICITY STARS

The Fe-group relative abundances are very similar in our three main-sequence turnoff stars with metallicities $[\text{Fe}/\text{H}] \simeq -2.9$. This is apparent from inspection of the $\log \epsilon$ and $[\text{X}/\text{H}]$ values in Table 3.

Unsurprisingly this abundance similarity extends to the $[\text{X}/\text{Fe}]$ values that are shown in Table 4. **These numbers are computed from the $[\text{X}/\text{H}]$ and $[\text{Fe}/\text{H}]$ values in Table 3.** The star-to-star variations in $[\text{X I}/\text{Fe}]$ and $[\text{X II}/\text{Fe}]$ are usually $\lesssim 0.1$ dex. The agreement among the three stars can also be seen by inspection of small spectral regions, as we illustrate in Figure 3. In this figure the line strengths for CD-33°1173 are weaker than those of the other two stars, due to its lower metallicity and substantially higher T_{eff} . But the ratios of depths of the Sc II and Co II lines compared to those of Fe II does not change much among the stars, nor do the line depths of other species not shown in this figure. Therefore we also have tabulated the three-star means of these values in this table; they serve as good representations for our final species abundances of our program stars.

For the elements Cr, Mn, and Cu, Table 4 has double entries for the neutral species abundances. As discussed in §3.1, both observational and theoretical (NLTE) evidence for Cr and Mn strongly suggests that their $\chi = 0$ eV resonance lines are not well represented by LTE computations for metal-poor stars. LTE abundances from higher-excitation neutral species transitions are more in accord with the abundances from the ionized species for these elements. Therefore the Table 4 labeled “Cr-rev” and “Mn-rev” contain the neutral-species abundances without inclusion of their resonance lines.

For Cu, NLTE studies agree that major upward abundance corrections are needed. Unfortunately, for Cu in our stars we have neither high-excitation Cu I nor Cu II transitions to provide observational guidance. Therefore for the neutral-species abundances in the row labeled “Cu-rev” we have applied an offset of $+0.50$ dex to the observed Cu abundances. We emphasize that this shift is an arbitrary single value. It probably is approximately correct, but it should be viewed with much caution.

In Figure 4 we display our final elemental abundance ratios **for our target stars. Most of the illustrated values are the means (ions and neutrals, where they both have been**

measured) taken from the last column of Table 4, except for cobalt where we have opted to use Co II. Also illustrated are abundance determinations for HD 84937 from SN16. Except for Cu and Zn the error bars in this figure represent the means of the scatters (sigmas). More definitive values for these error bars will only be possible with additional NLTE studies. For Cu and Zn there are not enough points to assess realistic scatter uncertainties, so we have assigned ± 0.15 to them. (This is consistent with the few sigma values obtained for these two elements, as shown in Table 3.) The most obvious departure from Solar abundances is the coordinated large overabundant element set of Sc, Ti, and V. In the next section we argue that this Fe-group abundance signature exists in larger spectroscopic surveys as well.

5. FE-GROUP ABUNDANCE RATIOS IN THE TARGET STARS AND OTHER LOW-METALLICITY STARS

The main results of our Fe-group abundance study of three very metal-poor main sequence turnoff stars are as follows: (a) the $[X/Fe]$ values agree within the errors for all species in all stars; (b) the lightest Fe-group elements are clearly all overabundant, with $\langle [X/Fe] \rangle \sim +0.4$; and (c) the abundances derived from Co I lines are uniformly larger than those from Co II by about 0.4 dex. Among the other elements, we find that $[Cr/Fe] \simeq [Ni/Fe] \simeq 0.0$, and $[Mn/Fe] \simeq [Cu/Fe] \simeq -0.2$ after estimated NLTE corrections are applied (§3.1.5 and §3.1.9). Our Zn abundance is based on two very weak lines detected in BD+03°740 and BD−13°3442 but not in CD−33°1173; little weight should be given to our results for this element.

SN16 discovered coordinated relative abundances of Sc, Ti, and V in HD 84937. They suggested that these abundance correlations generally can be found among results from surveys of halo stars with $[Fe/H] \lesssim -2$. With even larger Sc-Ti-V relative overabundances found in our program stars, we revisit this issue here. In Figure 5 we plot $[Sc\ II/Fe\ II]$ versus $[Ti\ II/Fe\ II]$ from six major studies along with our results. Different panels of this figure contain data from Cayrel et al. (2004), Cohen et al. (2004, 2008), Barklem et al. (2005), Lai et al. (2008), Yong et al. (2013), and Roederer et al. (2014a). All data sets show positive correlations between Sc and Ti abundances, and our program stars fall within the general set of abundances in each survey shown in this figure.

The large surveys included in Figure 5 and figures to follow are based on optical data, and their spectra have variable S/N values. Thus their abundances usually are based on substantially fewer lines than those of our program stars and HD 84937. In particular, Barklem et al. (2005) gathered “snapshot” high-resolution spectra, with the primary goal of identifying r -process-rich metal-poor giants. They chose to use relatively short exposure times in order to observe a large set of stars (373). Their spectra had modest fluxes, with $\langle S/N \rangle \sim 50$. This led Barklem et al. to report fewer abundances of elements only represented by a small number of weak transitions (e.g., V) than those with a rich set of lines (e.g., Ti). Therefore we chose to eliminate stars for which they obtained spectra with $S/N < 35$, and those for which they derived abundances of Sc and Ti but not V. These two choices combined to produce the Barklem et al. sample with the highest probability of good abundances for this element trio. Additionally, the panel Figure 5 with Cohen et al. (2004, 2008) results do not show the correlated trends seen in other surveys. However, the earlier Cohen et al. paper included only main sequence stars, and the later Cohen et al. paper concentrated on stars with $[Fe/H] \lesssim -3.4$, making it difficult to measure many Sc II and especially V II lines. We regard the

Cohen et al. abundances to be consistent with those from the other surveys, which have usually more favorable line detection probabilities for these elements.

In Figure 6 we merge all of the data sets into an overall [Sc/Fe] vs. [Ti/Fe] correlation plot. Also shown for illustrative purposes is a solid black line at a 45° angle, placed to go through the mean of our [Sc/Fe] values for HD 84937, BD+03°740, BD−13°3442, and CD−33°1173. All of the individual data sets, obtained with different atmospheric models, atomic line sets, and abundance techniques, cluster along this line, indicating a strong abundance correlation between these two elements. We have chosen not to apply additive constants to individual survey results in order to tighten the overall trend, because that would not materially change what is clear in this figure. That is, [Sc/Fe] and [Ti/Fe] vary in concert over a range of ~ 0.5 dex in individual very metal-poor ($[\text{Fe}/\text{H}] \lesssim -2$) Galactic halo stars. Abundances for our program objects lie at the high end of these abundance ratios, but other surveys have found stars with even higher values.

We make a similar abundance comparison with [V/Fe] and [Ti/Fe] in Figure 7. As in Figure 6 our results are again shown as filled circles, and again we have placed the 45° trend line to pass through the mean values of our program stars and HD 84937. The other data sets are from Barklem et al. (2005), Lai et al. (2008), and Roederer et al. (2014a). The surveys of Cohen et al. (2004, 2008) and Yong et al. (2013) did not report abundances from either V I or V II lines, due to the general weakness of this element’s transitions in the optical spectral region. Indeed, the abundances from V II lines in Barklem et al. are based only on the line at 3951.9 Å, and Roederer et al. used only that line and one other at 4005.7 Å. Only the Lai et al. study used more V II lines, most found at blue wavelengths down to about 3500 Å. Therefore, we do not regard the ~ 0.1 dex offset between our abundances and those of other literature sources as significant. Clearly there is a direct correlation between [V/Fe] and [Ti/Fe] among all of the data sets shown in Figure 7. The three lightest Fe-group elements, Sc, Ti and V, are correlated in metal-poor halo stars, and thus appear to have a closely related nucleosynthetic origin.

As a check on whether this correlation extends to other iron-peak elements, we examine [Ti/Fe] versus [Ni/Fe], as illustrated in Figure 8. A similar comparison was made in SN16, albeit with more limited data. We again include the data sets of Cayrel et al. (2004), Barklem et al. (2005), Cohen et al. (2004, 2008), Lai et al. (2008), Yong et al. (2013), and Roederer et al. (2014a), along with our new precise abundance values for low-metallicity stars. Figure 8 shows that Ti abundances are not correlated with Ni abundances, unlike the case of correlated Sc, Ti, and V abundances.

5.1. Nucleosynthesis Origins of the Fe-group elements

The production of Ti and V in core-collapse supernovae (CCSNe) has been studied in detail (see, e.g., discussion and references in Woosley & Weaver 1995). Explosive stellar yields are also available for different metallicities (e.g., Woosley & Weaver 1995; Limongi et al. 2000; Rauscher et al. 2002; Heger & Woosley 2010; Chieffi & Limongi 2013; Nomoto et al. 2013; Pignatari et al. 2016; Curtis et al. 2019). These iron-group elements are synthesized in the inner layers of stars undergoing complete or **incomplete silicon burning**. The production of these elements is tied to the explosion energies and details of the mass cut, which determines how much material is ejected in the explosion. Thus, in CCSNe ejecta, Ti and V are synthesized in the complete Si burning regions, but both elements tend to be underproduced relative to the observed abundance data for metal-poor halo stars. **Curtis et al. discuss production of Sc, Ti and V in detail. A couple of points from that work are worth mentioning here. First, Sc production can be complicated in these explosions,**

but it is mostly produced as Ti in the inner layers of the explosion. Second, although past spectroscopic results have linked Ti to α elements such as Mg, Si, and Ca, due to its relative overabundance, Ti is not a true α element (i.e., produced by the capture of α particles leading to stable isotopes with even numbers of protons and neutrons; e.g., ^{20}Ne and ^{40}Ca). Instead, Ti has a similar origin to Sc and V, and it is synthesized in Si burning regions deep in CCSNe, with the dominant Ti isotope being ^{48}Ti formed from the decay of ^{48}Cr .

In the future it will be important to make further precise abundance determinations in the metal-poor halo stars utilizing the new atomic laboratory data for the iron-peak elements. X. Ou et al. (in prep.) present a new reanalysis of the V abundances of nearly 300 stars in the Roederer et al. (2014a) sample. That study makes use of improved atomic data for V I (Lawler et al. 2014) and V II (Wood et al. 2014a) to expand the number of lines useful for a V abundance analysis, resulting in smaller abundance uncertainties and more stars with V detections. That study supports the results of SN16 and the present work that Sc, Ti, and V abundances are correlated in metal-poor stars.

5.2. Implications for Early Galactic Nucleosynthesis

In Figure 9 we show the [Ti/Fe] abundance ratios for our target stars (shown as filled circles) as a function of metallicity. Also illustrated are the derived abundances from other low-metallicity star surveys: Roederer et al. (2014a) (filled squares), Yong et al. (2013) (filled diamonds), Boesgaard et al. (2011) (plus signs), and Cohen et al. (2004, 2008) (filled right-facing triangles). It is clear that the values of [Ti/Fe] for our target stars are high, approaching +0.5, significantly higher than the solar value. In fact the data from all of the surveys indicates that [Ti/Fe] is substantially enhanced in low-metallicity stars. This trend has been reported before (SN16), but these new precise abundance values based on new laboratory atomic data for the three very low-metallicity target stars strongly support this result. We also note that recent work has suggested this trend continues at even lower metallicities, as Nordlander et al. (2019) report a value of [Ti/Fe] = +0.82 for a star with a metallicity of -6.2 .

These results suggest that at early Galactic times the synthesis sites for iron-peak element production make an overabundance of Ti. While CCSNe models have difficulty producing enhanced Ti (see discussion in SN16), higher explosion energies in hypernovae can produce larger amounts of certain iron-peak elements (Umeda & Nomoto 2002; Kobayashi et al. 2006). Galactic chemical evolution models (e.g., Kobayashi et al. 2006, 2011) that assume a 50% hypernova fraction can reproduce the overall abundance trends, but they have difficulty in achieving the actual abundance values seen in the data. These comparisons suggest that an even larger proportion of hypernovae might occur at very low metallicities and early in the history of the Galaxy (cf. Ezzeddine et al. 2019).

As noted above in §3.1, early surveys, employing only neutral Co abundances, indicated overabundances of [Co/Fe] at low metallicities. We examine the abundance trends of [Co/Fe] in Figure 10 using data from Lai et al. (2008), Roederer et al. (2014a), SN16, and our new abundance determinations for the three low metallicity target stars. In general the data are not consistent with an overabundance at low metallicities. The exceptions are the new values for our target stars when employing abundances derived only the neutral (minority) species, which are significantly larger than the abundances derived from Co II lines. It is also clear in the figure that both neutral and ionized species of Co give the same result for the somewhat more metal-rich HD 84937 (SN16). We conclude that the [Co/Fe] abundance ratios derived from singly-ionized Co are correct, and that differences

between the neutral and ionized results are mostly likely due to NLTE effects. Clearly, this issue should be examined in the future.

As a final iron-peak element abundance comparison, we examine the chemical evolution of $[\text{Ni}/\text{Fe}]$ in Figure 11. Our new abundance determinations for the program stars, along with data from Cayrel et al. (2004), Cohen et al. (2004, 2008), Lai et al. (2008), Yong et al. (2013), and Roederer et al. (2014a), indicate mostly solar values of $[\text{Ni}/\text{Fe}]$ over a large metallicity range.

6. SUMMARY AND CONCLUSIONS

We have determined new precise abundances for the iron-peak elements (Sc–Zn) in three very metal-poor ($[\text{Fe}/\text{H}] \approx -3$) stars: BD+03°740, BD−13°3442, and CD−33°1173. Our high-resolution spectroscopic data sources include *HST*/STIS UV spectra and optical ground-based spectra from several sources. This is the first study of the complete set of Fe-group elements with recent, consistent lab data.

Comparing our new abundance values with other surveys, we conclude that the three lightest Fe-group elements, Sc, Ti, and V, are correlated in metal-poor halo stars. Our target stars fall on the high-end of this general, relatively unstudied correlation. It has been reported previously that the iron-peak elements Sc, V, and especially Ti are often overabundant in stars at low metallicities. Our new abundance results for these three metal-poor halo stars strongly support this finding. These results suggest a similar astrophysical origin for these three elements and place strong constraints on early Galactic nucleosynthesis and CCSNe models. Previous Galactic chemical evolution models employing various proportions of CCSNe have had difficulty in achieving the observed levels of Ti. Our work might suggest more energetic CCSNe, i.e., hypernovae, could have been more common, and thus responsible for this synthesis early in the history of the Galaxy.

Finally, our detailed neutral and ionized Co abundance measurements indicate that there are overabundances only when studying Co I lines. We suggest that $[\text{Co}/\text{Fe}]$ values given by the ionized species are correct and there are no overabundances of this iron-peak element in very low-metallicity stars.

We thank our colleagues for help and advice, including X. Ou. **We are also grateful to the referee for providing useful comments that helped improve this paper.** This work has been supported in part by NASA grant NNX16AE96G (J.E.L.), by National Science Foundation (NSF) grants AST-1516182 and AST-1814512 (J.E.L. and E.D.H.), AST-1616040 (C.S.) and AST-1613536 and AST-1815403 (IUR). JJC and IUR were supported in part by the JINA Center for the Evolution of the Elements, supported by the NSF under Grant No. PHY-1430152.

Facility: HST (STIS), Keck I (HIRES), McDonald 2.7m Smith (Tull), VLT (UVES)

Software: **linemake** (<https://github.com/vmplacco/linemake>), **MOOG** (Snedden 1973; Sobeck et al. 2011)

REFERENCES

- Andrievsky, S., Bonifacio, P., Caffau, E., et al. 2018, *MNRAS*, 473, 3377
- Asplund, M., Grevesse, N., Sauval, A. J., & Scott, P. 2009, *ARA&A*, 47, 481
- Barklem, P. S., Christlieb, N., Beers, T. C., et al. 2005, *A&A*, 439, 129
- Bergemann, M., & Gehren, T. 2008, *A&A*, 492, 823
- Bergemann, M., Pickering, J. C., & Gehren, T. 2010, *MNRAS*, 401, 1334
- Boesgaard, A. M., Rich, J., Levesque, E. M., & Bowler, B. P. 2011, *ApJ*, 743, 140
- Bonifacio, P., Molaro, P., Sivarani, T., et al. 2007, *A&A*, 462, 851
- Cayrel, R., Depagne, E., Spite, M., et al. 2004, *A&A*, 416, 1117
- Chieffi, A., & Limongi, M. 2013, *ApJ*, 764, 21
- Cohen, J. G., Christlieb, N., McWilliam, A., et al. 2008, *ApJ*, 672, 320
- . 2004, *ApJ*, 612, 1107
- Cowan, J. J., Sneden, C., Lawler, J. E., et al. 2019, arXiv e-prints, arXiv:1901.01410
- Curtis, S., Ebinger, K., Frohlich, C., et al. 2019, *ApJ*, 870, 2
- Dekker, H., D’Odorico, S., Kaufer, A., Delabre, B., & Kotzłowski, H. 2000, in *Society of Photo-Optical Instrumentation Engineers (SPIE) Conference Series*, Vol. 4008, *Proc. SPIE*, ed. M. Iye & A. F. Moorwood, 534–545
- Den Hartog, E. A., Lawler, J. E., Sneden, C., Cowan, J. J., & Brukhovesky, A. 2019, *ApJS*, 243, 33
- Den Hartog, E. A., Lawler, J. E., Sobeck, J. S., Sneden, C., & Cowan, J. J. 2011, *ApJS*, 194, 35
- Ezzeddine, R., Frebel, A., Roederer, I. U., et al. 2019, *ApJ*, 876, 97
- Fedchak, J. A., & Lawler, J. E. 1999, *ApJ*, 523, 734
- Grevesse, N., Scott, P., Asplund, M., & Sauval, A. J. 2015, *A&A*, 573, A27
- Heger, A., & Woosley, S. E. 2010, *ApJ*, 724, 341
- Hosford, A., Ryan, S. G., García Pérez, A. E., Norris, J. E., & Olive, K. A. 2009, *A&A*, 493, 601
- Kimble, R. A., Woodgate, B. E., Bowers, C. W., et al. 1998, *ApJL*, 492, L83
- Kobayashi, C., Karakas, A. I., & Umeda, H. 2011, *MNRAS*, 414, 3231
- Kobayashi, C., Umeda, H., Nomoto, K., Tominaga, N., & Ohkubo, T. 2006, *ApJ*, 653, 1145
- Kramida, A., Yu. Ralchenko, Reader, J., & and NIST ASD Team. 2018, *NIST Atomic Spectra Database (ver. 5.6.1)*, [Online]. Available: <https://physics.nist.gov/asd> [2016, January 31]. National Institute of Standards and Technology, Gaithersburg, MD.
- Kurucz, R. L. 2011, *Canadian Journal of Physics*, 89, 417
- Lai, D. K., Bolte, M., Johnson, J. A., et al. 2008, *ApJ*, 681, 1524
- Lawler, J. E., Feigenson, T., Sneden, C., Cowan, J. J., & Nave, G. 2018, *ApJS*, 238, 7
- Lawler, J. E., Guzman, A., Wood, M. P., Sneden, C., & Cowan, J. J. 2013, *ApJS*, 205, 11
- Lawler, J. E., Hala, Sneden, C., et al. 2019, *ApJS*, 241, 21
- Lawler, J. E., Sneden, C., & Cowan, J. J. 2015, *ApJS*, 220, 13
- Lawler, J. E., Sneden, C., Cowan, J. J., Ivans, I. I., & Den Hartog, E. A. 2009, *ApJS*, 182, 51
- Lawler, J. E., Sneden, C., Nave, G., et al. 2017, *ApJS*, 228, 10
- Lawler, J. E., Wood, M. P., Den Hartog, E. A., et al. 2014, *ApJS*, 215, 20
- Limongi, M., Straniero, O., & Chieffi, A. 2000, *ApJS*, 129, 625
- McWilliam, A., Preston, G. W., Sneden, C., & Searle, L. 1995, *AJ*, 109, 2757
- Meléndez, J., & Barbuy, B. 2009, *A&A*, 497, 611
- Nomoto, K., Kobayashi, C., & Tominaga, N. 2013, *ARA&A*, 51, 457
- Nordlander, T., Bessell, M. S., Da Costa, G. S., et al. 2019, *MNRAS*, 488, L109
- Pignatari, M., Herwig, F., Hirschi, R., et al. 2016, *ApJS*, 225, 24
- Rauscher, T., Heger, A., Hoffman, R. D., & Woosley, S. E. 2002, *ApJ*, 576, 323
- Roederer, I. U., & Barklem, P. S. 2018, *ApJ*, 857, 2
- Roederer, I. U., Preston, G. W., Thompson, I. B., et al. 2014a, *AJ*, 147, 136
- Roederer, I. U., Sneden, C., Lawler, J. E., et al. 2018, *ApJ*, 860, 125

- Roederer, I. U., Schatz, H., Lawler, J. E., et al. 2014b, *ApJ*, 791, 32
- Ryan, S. G., Norris, J. E., & Beers, T. C. 1996, *ApJ*, 471, 254
- . 1999, *ApJ*, 523, 654
- Ryan, S. G., Norris, J. E., & Bessell, M. S. 1991, *AJ*, 102, 303
- Shi, J. R., Yan, H. L., Zhou, Z. M., & Zhao, G. 2018, *ApJ*, 862, 71
- Sneden, C. 1973, *ApJ*, 184, 839
- Sneden, C., Cowan, J. J., Kobayashi, C., et al. 2016, *ApJ*, 817, 53
- Sneden, C., Lawler, J. E., Cowan, J. J., Ivans, I. I., & Den Hartog, E. A. 2009, *ApJS*, 182, 80
- Sobeck, J. S., Lawler, J. E., & Sneden, C. 2007, *ApJ*, 667, 1267
- Sobeck, J. S., Kraft, R. P., Sneden, C., et al. 2011, *AJ*, 141, 175
- Tull, R. G., MacQueen, P. J., Sneden, C., & Lambert, D. L. 1995, *PASP*, 107, 251
- Umeda, H., & Nomoto, K. 2002, *ApJ*, 565, 385
- Vogt, S. S., Allen, S. L., Bigelow, B. C., et al. 1994, in *Society of Photo-Optical Instrumentation Engineers (SPIE) Conference Series*, Vol. 2198, *Instrumentation in Astronomy VIII*, ed. D. L. Crawford & E. R. Craine, 362
- Wallerstein, G., & Helfer, H. L. 1959, *ApJ*, 129, 720
- Wood, M. P., Lawler, J. E., Den Hartog, E. A., Sneden, C., & Cowan, J. J. 2014a, *ApJS*, 214, 18
- Wood, M. P., Lawler, J. E., Sneden, C., & Cowan, J. J. 2013, *ApJS*, 208, 27
- . 2014b, *ApJS*, 211, 20
- Wood, M. P., Sneden, C., Lawler, J. E., et al. 2018, *ApJS*, 234, 25
- Woodgate, B. E., Kimble, R. A., Bowers, C. W., et al. 1998, *PASP*, 110, 1183
- Woolsey, S. E., & Weaver, T. A. 1995, *ApJS*, 101, 181
- Yong, D., Norris, J. E., Bessell, M. S., et al. 2013, *ApJ*, 762, 26
- Yousefi, M., & Bernath, P. F. 2018, *ApJS*, 237, 8

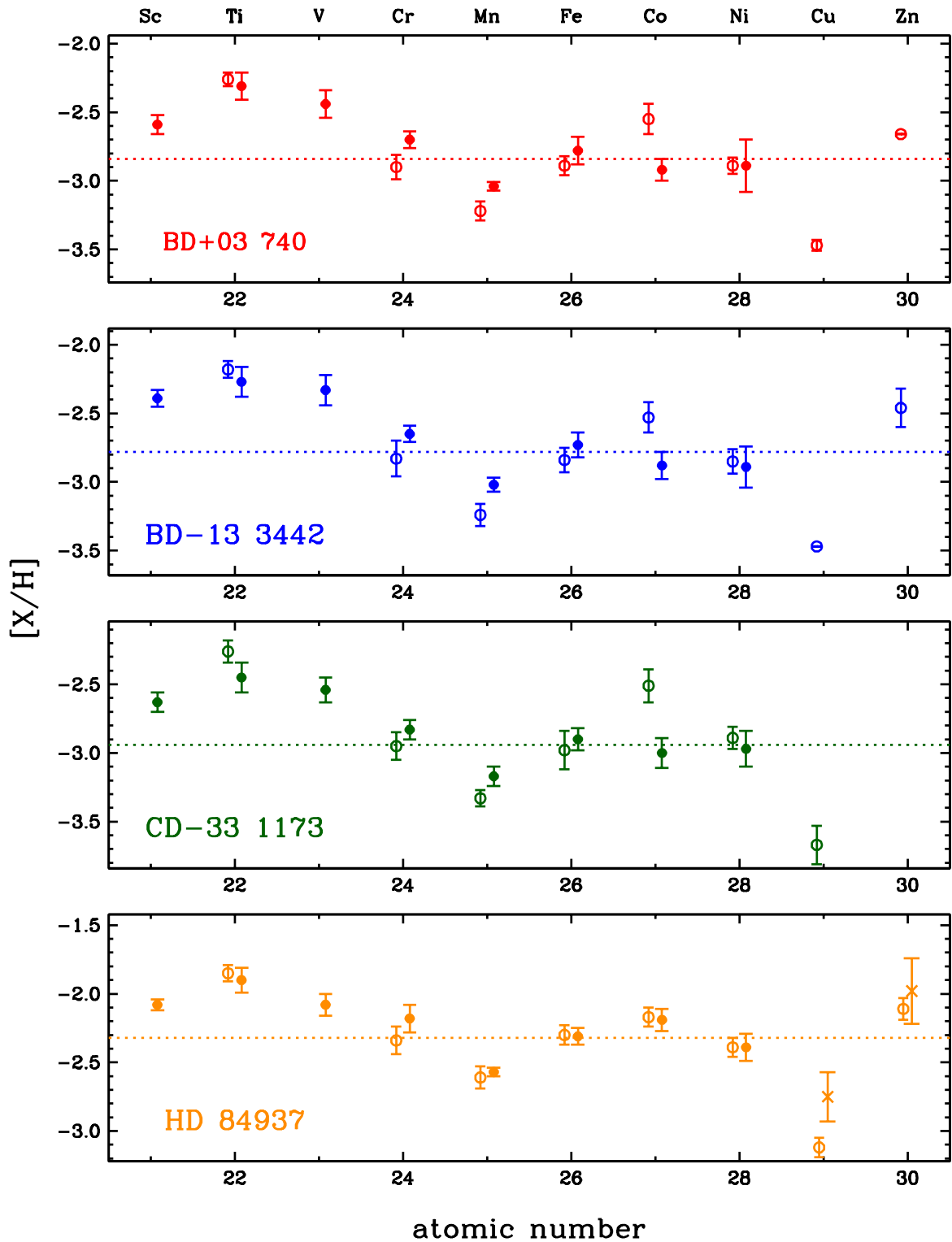


Figure 1. Abundance ratios $[X/H]$ for the three program stars and for HD 84937. In each panel the dotted line represents the mean $[\text{Fe}/\text{H}]$ for that star. The abundances derived from neutral-species transitions are shown as open circles, and they are shifted slightly to the right of their atomic numbers. The abundances from ionized-species transitions are shown as filled circles and shifted slightly to the left. In the panel for HD 84937, we show the Cu II and Zn II abundances from Roederer & Barklem (2018) as \times symbols. The error bars here are the sample standard deviation σ values from Table 3 for each species abundance.

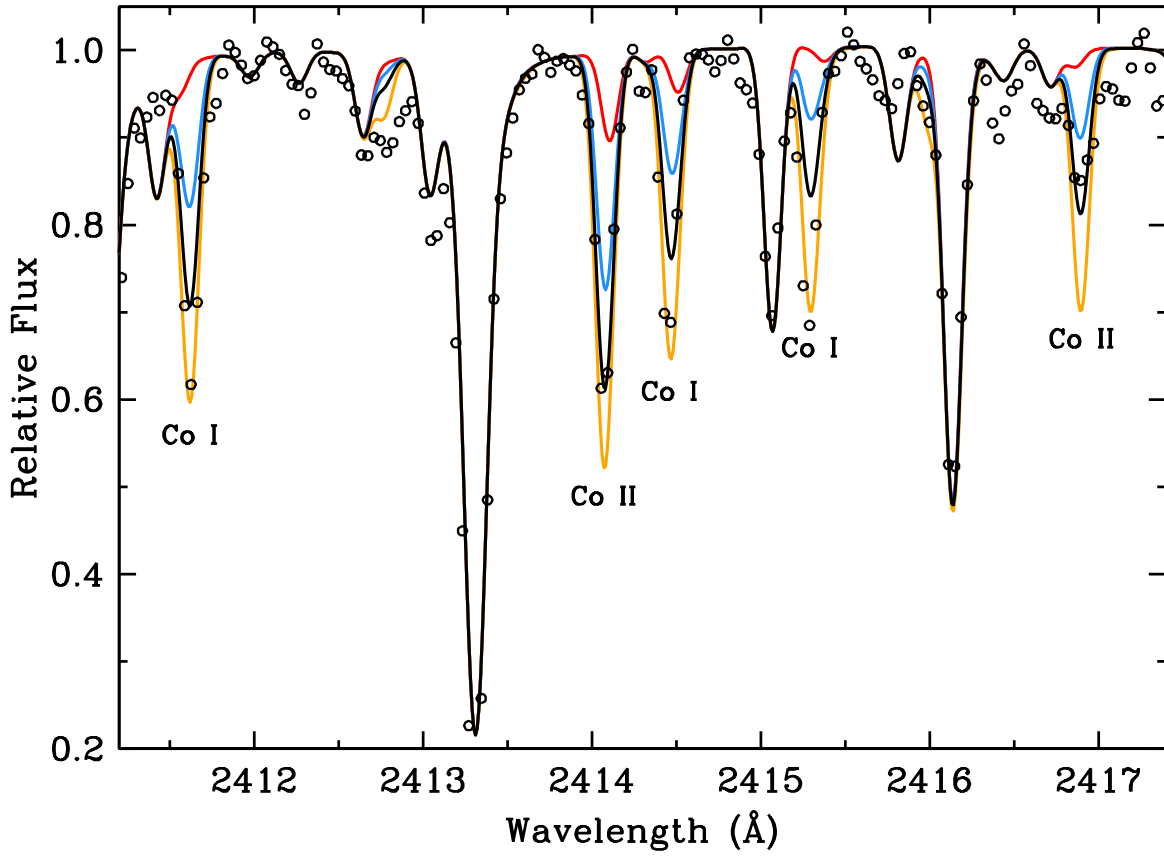


Figure 2. Observed spectra (open circles) and syntheses (lines) in a small spectral region with both for Co I and Co II transitions. For the syntheses, the red color indicates what the spectrum would look like with no Co contribution and the black color is for the mean Co abundance from Co II features. The blue and orange lines represent the Co II-based abundance decreased and increased by 0.4 dex.

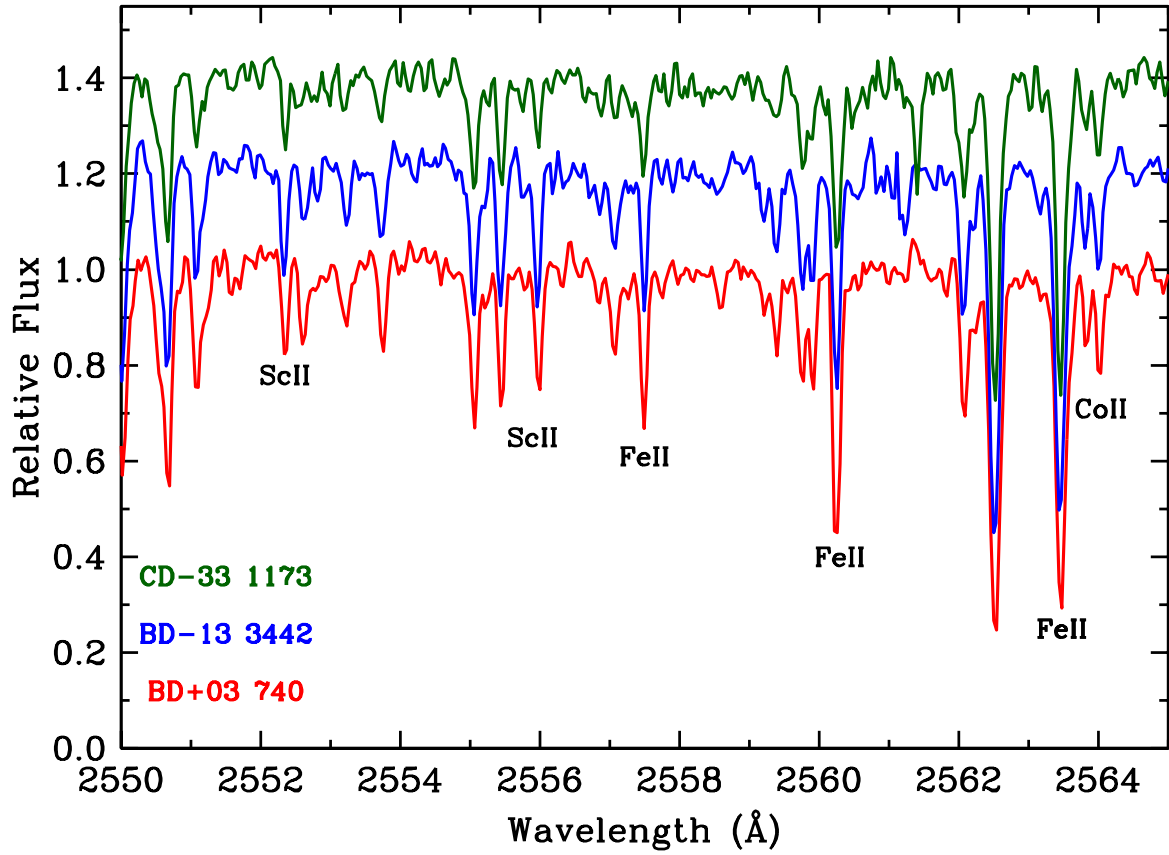


Figure 3. Spectra of the three program stars in a small UV region. Essentially all of the absorption features can be accounted for by Fe-group transitions, some of which are labeled in the figure. For clarity the relative flux scales for BD-13°3442 and CD-33°1173 have been shifted by +0.2 and +0.4, respectively.

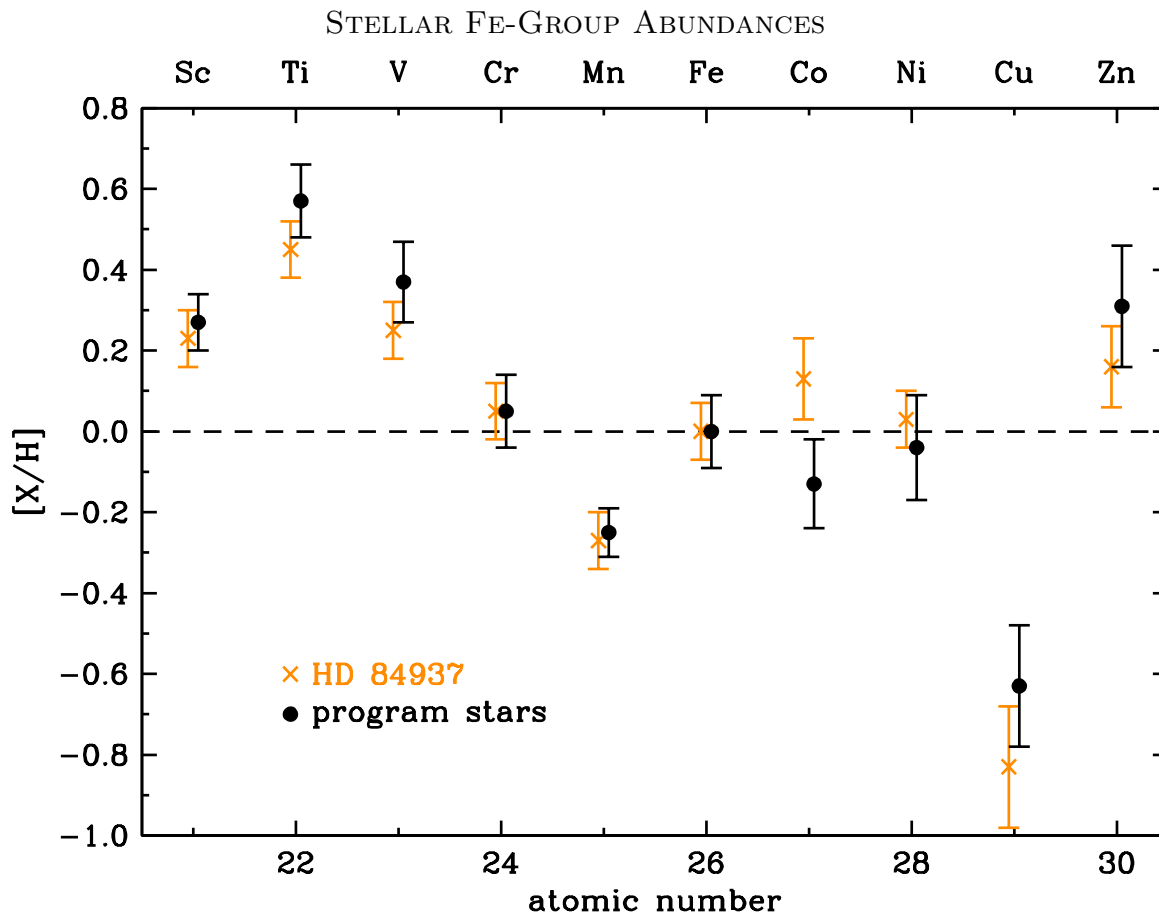


Figure 4. Final elemental relative abundance ratios for the three program stars. See §4 for explanations of the chosen ratios and the associated error bars. The relative abundance ratios for HD 84937 (SN16) are also shown in the figure.

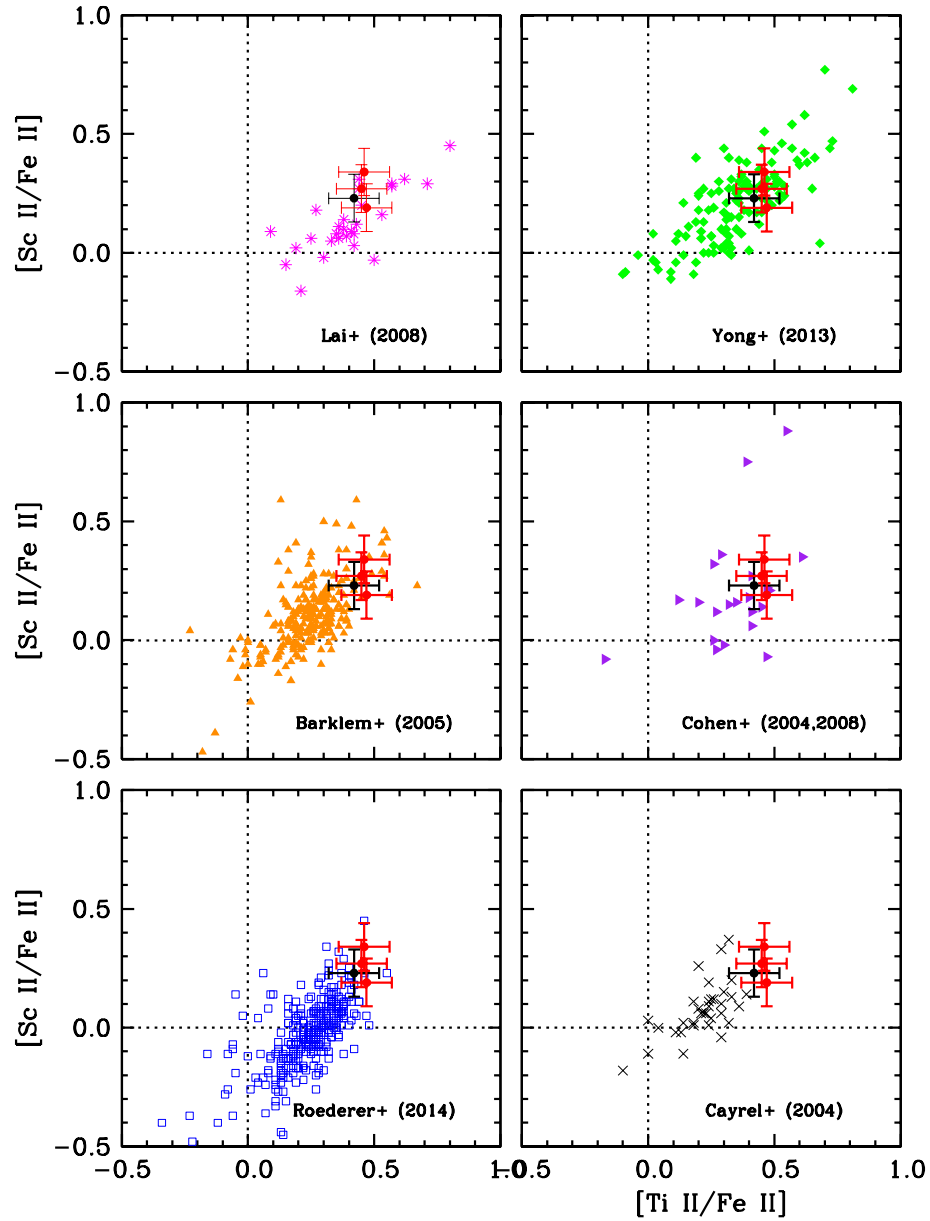


Figure 5. Correlations of $[\text{Sc}/\text{Fe}]$ and $[\text{Ti}/\text{Fe}]$ ratios in six major halo-star abundance surveys, Cayrel et al. (2004), Cohen et al. (2004, 2008), Barklem et al. (2005), Lai et al. (2008), Yong et al. (2013), and Roederer et al. (2014a). In each panel the HD 84937 value from SN16 is shown as a black dot with error bars, and the three program stars are red dots with error bars.

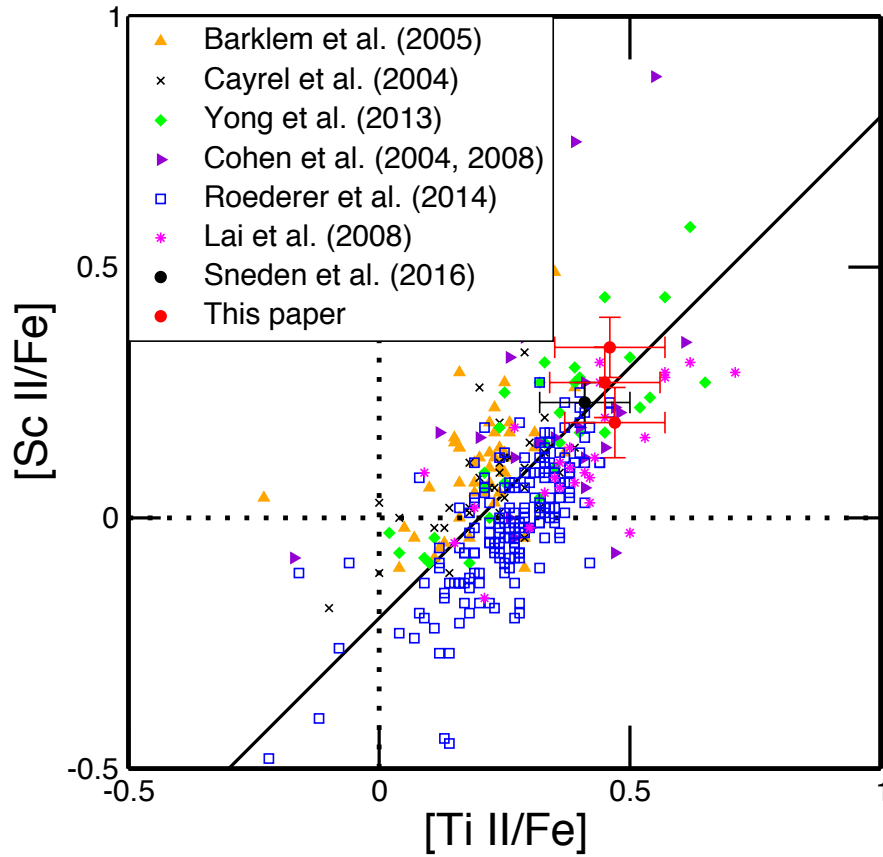


Figure 6. Abundance ratios $[\text{Sc}/\text{Fe}]$ versus $[\text{Ti}/\text{Fe}]$ from ionized transitions of each element. The open squares are from Roederer et al. (2014a), filled diamonds from Yong et al. (2013), filled right-facing triangles from Cohen et al. (2004, 2008), filled upward-facing triangles from Barklem et al. (2005), x's are from Cayrel et al. (2004), stars from Lai et al. (2008) and the filled circles for BD+03°740, BD−13°3442, CD−33°1173, and HD 84937 derived in this paper or in SN16. The horizontal and vertical (dotted) lines denote the solar abundance ratios of each element. The solid line represents a 45° slope.

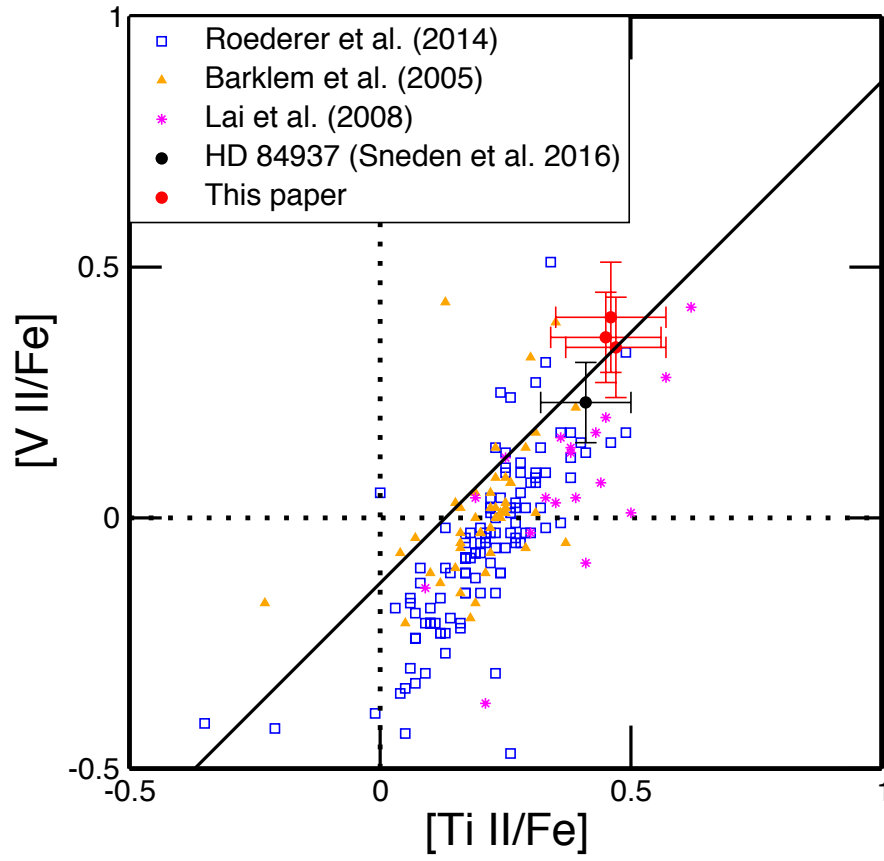


Figure 7. Abundance ratios $[V/Fe]$ versus $[Ti/Fe]$ from ionized transitions of each element. The symbols are as in Figure 6.

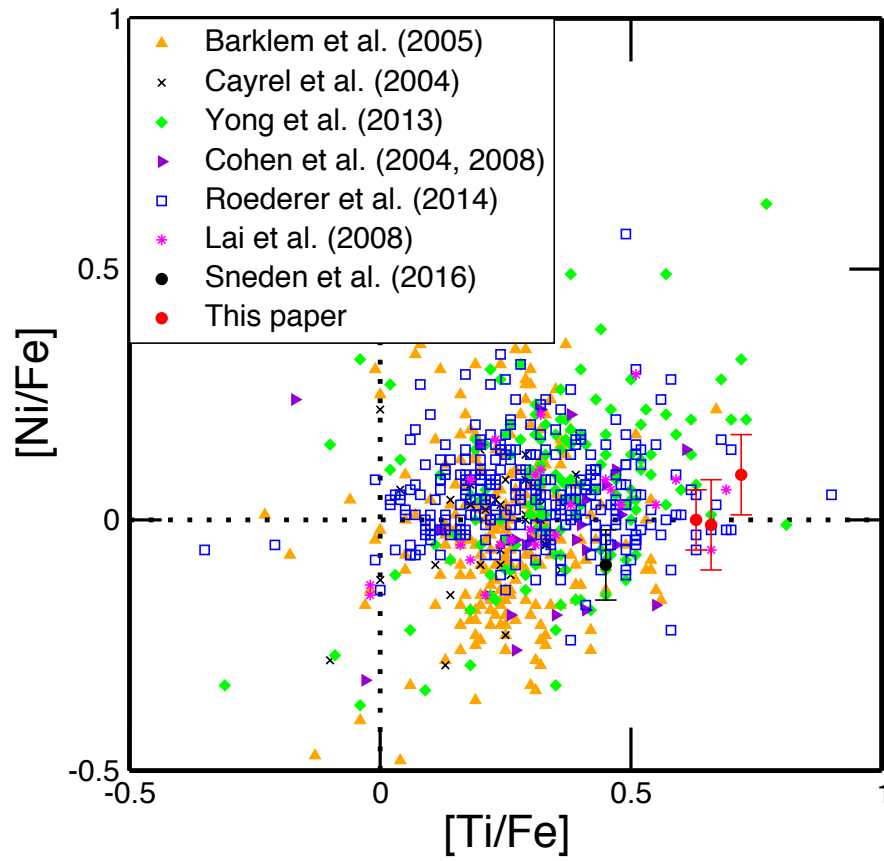


Figure 8. Abundance ratios $[\text{Ni}/\text{Fe}]$ versus $[\text{Ti}/\text{Fe}]$ from neutral transitions of each element. The symbols are as in Figure 6.

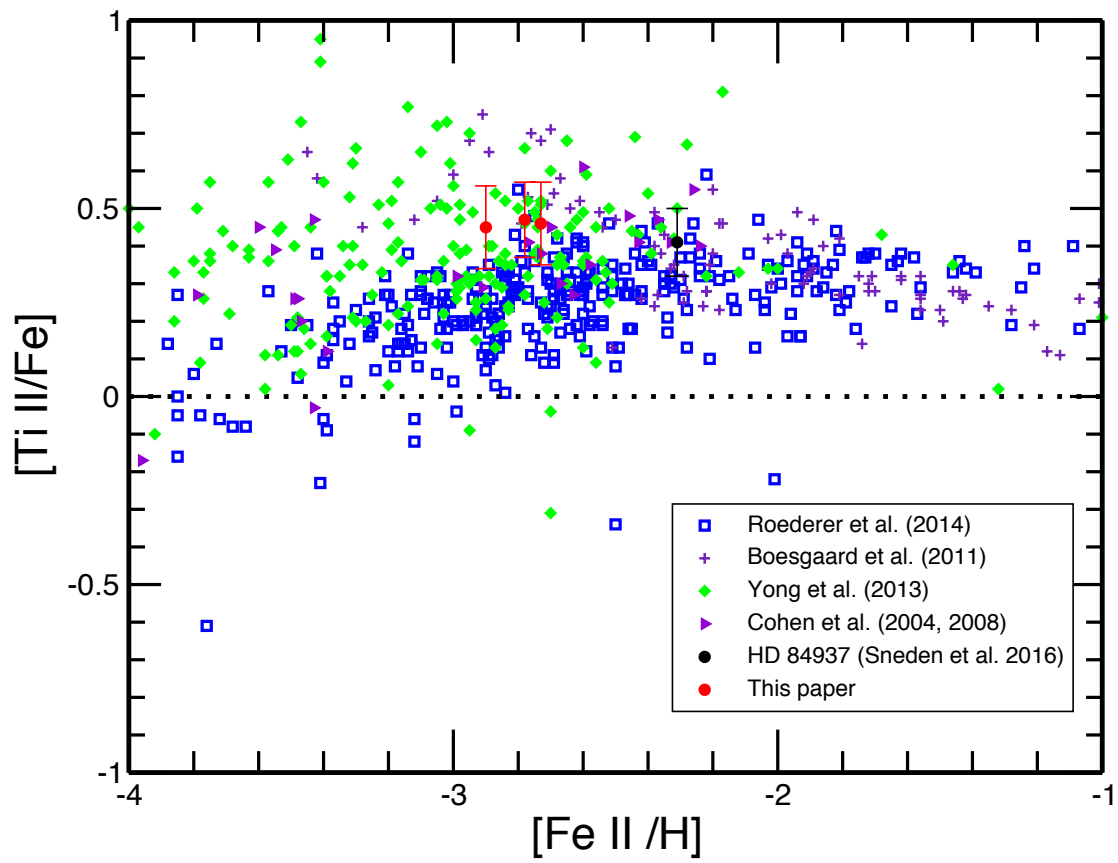


Figure 9. Abundance ratios $[\text{Ti II}/\text{Fe}]$ plotted as function of $[\text{Fe II}/\text{H}]$ metallicity. The symbols are as in Figure 6 with plus signs from Boesgaard et al. (2011). See text for detailed discussion.

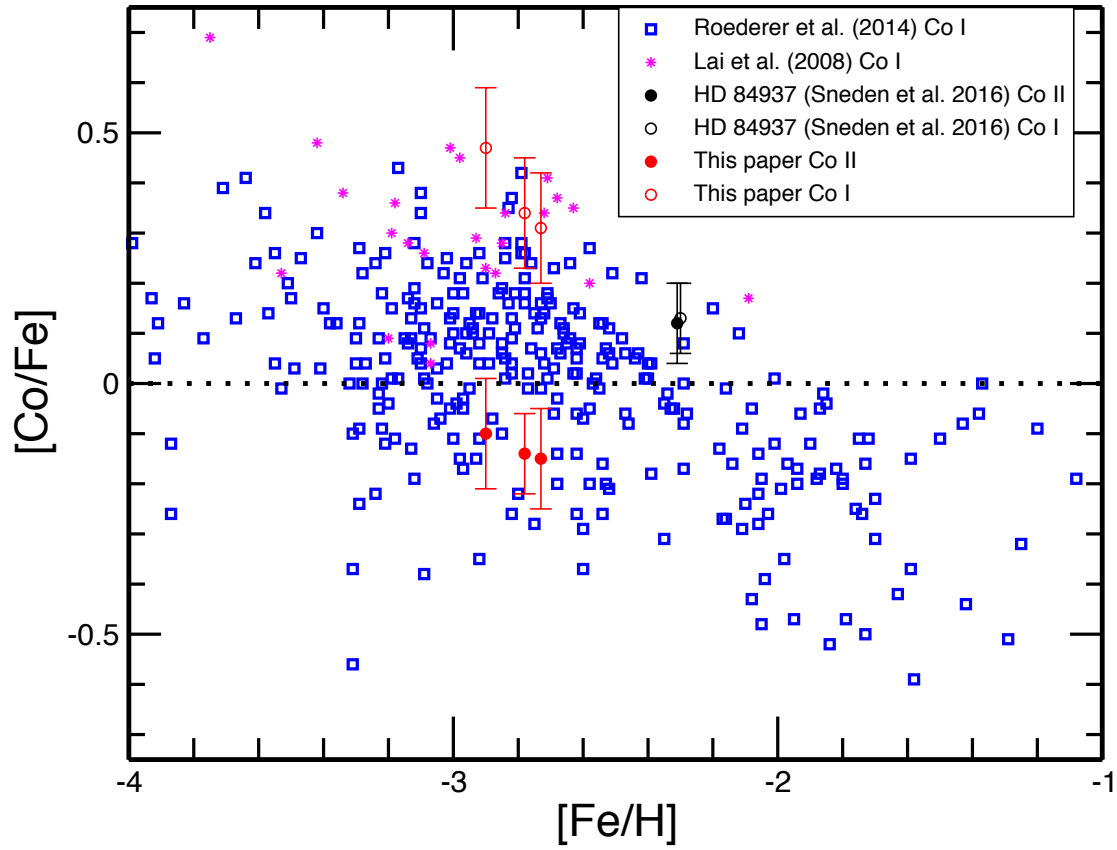


Figure 10. Abundance ratios $[\text{Co}/\text{Fe}]$ plotted as function of $[\text{Fe}/\text{H}]$ metallicity. The symbols are as in Figure 6. See text for detailed discussion.

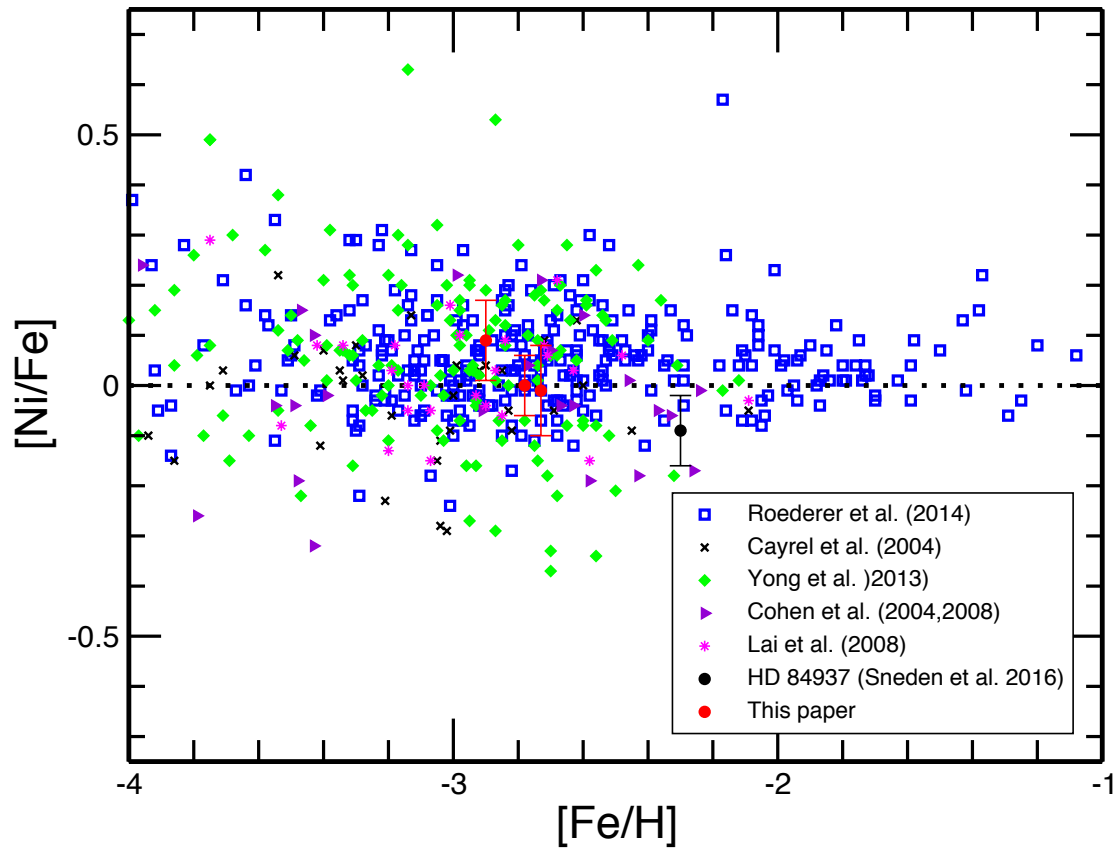


Figure 11. Abundance ratios $[\text{Ni}/\text{Fe}]$ plotted as function of $[\text{Fe}/\text{H}]$ metallicity. The symbols are as in Figure 6. See text for detailed discussion.

Table 1. Model Atmospheric Parameters

Star	T_{eff}	$\log g$	ξ_t	[M/H]
	K		km s ⁻¹	
BD+03°740	6351	3.97	1.70	-2.90
BD-13°3442	6405	4.04	1.60	-2.85
CD-33°1173	6625	4.29	1.60	-3.00
HD 84937	6300	4.00	1.50	-2.15

Table 2. Line Parameters and Abundances

λ	Species	χ	$\log gf$	$\log \epsilon$	$\log \epsilon$	$\log \epsilon$
\AA		eV		BD+03°740	BD−13°3442	CD−33°1173
2552.354	Sc II	0.022	0.05	0.50	0.65	0.45
2555.795	Sc II	0.000	−0.69	0.60	0.80	0.65
2563.190	Sc II	0.000	−0.57	0.40	0.75	...
3353.724	Sc II	0.315	0.26	0.58	0.75	0.52
3359.678	Sc II	0.008	−0.75	0.70	0.75	0.65
3361.931	Sc II	0.000	−0.72	0.65	0.85	0.65
3368.936	Sc II	0.008	−0.39	0.60	0.77	0.58
3535.714	Sc II	0.315	−0.46	0.55	0.75	0.50
3567.696	Sc II	0.000	−0.47	0.58	0.74	0.46
3572.526	Sc II	0.022	0.27	0.61	0.81	0.57
3576.340	Sc II	0.008	0.01	0.55	0.74	0.52
3580.925	Sc II	0.000	−0.14	0.55	0.74	0.48
3589.632	Sc II	0.008	−0.57	0.60	0.77	0.53

NOTE—The complete version of this table is available in the online edition of the journal. An abbreviated version is shown here to illustrate its form and content.

Table 3. Mean Abundances

El	Sun		BD+03°740				BD−13°3442				CD−33°1173			
	log ϵ	source	log ϵ	σ	num	[X/H]	log ϵ	σ	num	[X/H]	log ϵ	σ	num	[X/H]
Neutral Species														
Sc	3.15	1
Ti	4.97	2	2.71	0.05	24	−2.26	2.79	0.06	17	−2.18	2.71	0.08	10	−2.26
V	3.96	4
Cr	5.64	6	2.74	0.09	13	−2.90	2.81	0.13	12	−2.83	2.69	0.10	10	−2.95
Mn	5.45	8	2.23	0.07	5	−3.22	2.21	0.08	5	−3.24	2.12	0.06	3	−3.33
Fe	7.50	10	4.61	0.07	230	−2.89	4.66	0.09	243	−2.84	4.52	0.14	194	−2.98
Co	4.96	11	2.41	0.11	36	−2.55	2.43	0.11	31	−2.53	2.45	0.12	28	−2.51
Ni	6.28	13	3.39	0.06	45	−2.89	3.43	0.09	43	−2.85	3.39	0.08	35	−2.89
Cu	4.18	15	0.71	(0.1) ^a	2	−3.47	0.71	(0.1) ^a	2	−3.47	0.51	0.14	2	−3.67
Zn	4.56	15	1.90	(0.1) ^a	2	−2.66	2.10	0.14	2	−2.46
Ionized Species														
Sc	3.16	1	0.57	0.07	27	−2.59	0.77	0.06	27	−2.39	0.53	0.07	19	−2.63
Ti	4.98	3	2.67	0.10	108	−2.31	2.71	0.11	99	−2.27	2.53	0.11	72	−2.45
V	3.95	5	1.51	0.10	47	−2.44	1.62	0.11	41	−2.33	1.41	0.09	30	−2.54
Cr	5.62	7	2.92	0.06	50	−2.70	2.97	0.06	57	−2.65	2.79	0.07	56	−2.83
Mn	5.45	9	2.41	0.03	10	−3.04	2.43	0.05	6	−3.02	2.28	0.07	6	−3.17
Fe	7.50	10	4.72	0.10	68	−2.78	4.77	0.09	70	−2.73	4.60	0.08	61	−2.90
Co	4.96	12	2.04	0.08	21	−2.92	2.08	0.10	19	−2.88	1.96	0.11	16	−3.00
Ni	6.28	14	3.39	0.19	8	−2.89	3.39	0.15	8	−2.89	3.31	0.13	7	−2.97
Cu	4.18	16
Zn	4.61	16

^aThe formal σ value is unrealistically close to zero, so the table value is arbitrarily set to 0.1

References—The citations to solar abundance sources enumerated in the third column are: [1] Lawler et al. (2019); [2] Lawler et al. (2013); [3] Wood et al. (2013); [4] Lawler et al. (2014); [5] Wood et al. (2014a), [6] Sobeck et al. (2007); [7] Lawler et al. (2017); [8] Sneden et al. (2016); [9] assumed from the Mn I solar abundance (Sneden et al. 2016); [10] Asplund et al. (2009); [11] Lawler et al. (2015); [12] assumed from the Co I solar abundance (Lawler et al. 2015); [13] Wood et al. (2014b); [14] assumed from the Ni I abundance; [15] (Grevesse et al. 2015); [16] assumed from the Cu I and Zn I solar abundances (Grevesse et al. 2015).

Table 4. Final Abundance Ratios

El	[X I/Fe]	[X I/Fe]	[X I/Fe]	\langle [X I/Fe] \rangle	[X II/Fe]	[X II/Fe]	[X II/Fe]	\langle [X II/Fe] \rangle	\langle [X/Fe] \rangle
	BD+03°740	BD−13°3442	CD−33°1173		BD+03°740	BD−13°3442	CD−33°1173		El
Sc	0.19	0.34	0.27	0.27	0.27
Ti	0.63	0.66	0.72	0.67	0.47	0.46	0.45	0.46	0.57
V	0.34	0.40	0.36	0.37	0.37
Cr	−0.01	0.01	0.03	0.01	0.08	0.08	0.07	0.08	
Cr-rev ^a	0.04	0.11	0.00	0.05	0.06
Mn	−0.33	−0.40	−0.35	−0.36	−0.26	−0.29	−0.27	−0.27	
Mn-rev ^b	−0.16	−0.22	−0.27	−0.22	−0.25
Fe	0.00	0.00	0.00	0.00	0.00	0.00	0.00	0.00	0.00
Co	0.34	0.31	0.47	0.37	−0.14	−0.15	−0.10	−0.13	−0.13
Ni	0.00	−0.01	0.09	0.03	−0.11	−0.16	−0.07	−0.11	0.03
Cu	−0.58	−0.63	−0.69	−0.63	
Cu-rev ^c	−0.08	−0.13	−0.19	−0.13	−0.13
Zn	0.23	0.38	...	0.31	0.31

^aCr-rev is the Cr I abundance neglecting the transitions arising from the 0 eV ground state

^bMn-rev is the Mn I abundance neglecting the transitions arising from the 0 eV ground state

^cCu-rev is the Cu I abundance with the addition of 0.5 dex, roughly approximating an NLTE correction